Quasiparticle lifetime of the repulsive Fermi polaron

Haydn S. Adlong,[1] Weizhe Edward Liu,[1, 2] Francesco Scazza,[3] Matteo Zaccanti,[3]
Nelson Darkwah Oppong,[4, 5, 6] Simon Fölling,[4, 5, 6] Meera M. Parish,[1, 2] and Jesper Levinsen[1, 2]

[1]*School of Physics and Astronomy, Monash University, Victoria 3800, Australia.*
[2]*ARC Centre of Excellence in Future Low-Energy Electronics Technologies, Monash University, Victoria 3800, Australia*
[3]*Istituto Nazionale di Ottica del Consiglio Nazionale delle Ricerche (CNR-INO) and*
European Laboratory for Nonlinear Spectroscopy (LENS), 50019 Sesto Fiorentino, Italy
[4]*Ludwig-Maximilians-Universität, Schellingstraße 4, 80799 München, Germany*
[5]*Max-Planck-Institut für Quantenoptik, Hans-Kopfermann-Straße 1, 85748 Garching, Germany*
[6]*Munich Center for Quantum Science and Technology (MCQST), Schellingstraße 4, 80799 München, Germany*
(Dated: September 9, 2020)

We investigate the metastable repulsive branch of a mobile impurity coupled to a degenerate Fermi gas via short-range interactions. We show that the quasiparticle lifetime of this repulsive Fermi polaron can be experimentally probed by driving Rabi oscillations between weakly and strongly interacting impurity states. Using a time-dependent variational approach, we find that we can accurately model the impurity Rabi oscillations that were recently measured for repulsive Fermi polarons in both two and three dimensions. Crucially, our theoretical description does not include relaxation processes to the lower-lying attractive branch. Thus, the theory-experiment agreement demonstrates that the quasiparticle lifetime is dominated by many-body dephasing within the upper repulsive branch rather than by relaxation from the upper branch itself. Our findings shed light on recent experimental observations of persistent repulsive correlations, and have important consequences for the nature and stability of the strongly repulsive Fermi gas.

The concept of the quasiparticle is a powerful tool for describing interacting many-body quantum systems. Most notably, it forms the basis of Fermi liquid theory [1], a highly successful phenomenological description of interacting Fermi systems ranging from liquid ^{3}He to electrons in semiconductors. Here, the underlying particles are "dressed" by many-body excitations to form weakly interacting quasiparticles with modified properties such as a finite lifetime and an effective mass. However, during the past few decades, many materials have emerged that defy a conventional explanation within Fermi liquid theory [2, 3]. Therefore, it is important to understand how quasiparticles can lose their coherence or break down.

Quantum impurities in quantum gases provide an ideal testbed in which to investigate quasiparticles since the impurity-medium interactions can be tuned to controllably create dressed impurity particles or *polarons* [4]. To date, there have been a multitude of successful cold-atom experiments on impurities coupled to Fermi [5–17] and Bose [18–22] gases, which are termed Fermi and Bose polarons, respectively. In particular, Fermi-polaron experiments have observed the real-time formation of quasiparticles [13] and the disappearance of quasiparticles in the spectral response with increasing temperature [15]. The Fermi-polaron scenario has even been extended beyond cold atoms, having recently been realized in charge-tunable atomically thin semiconductors [23]. While the ground state of the Fermi polaron (corresponding to the attractive branch) is generally well understood [24–32], there has been much debate about the nature of the metastable repulsive branch [30, 33–38], with experiments suggesting that it can be remarkably long-lived for a range of interactions [7, 14, 16]. The stability of
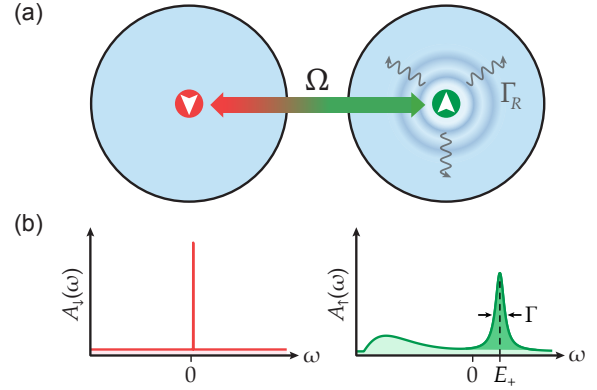

FIG. 1. (a) Two pseudo-spin states (red and green) of an impurity embedded in a medium (blue) are coupled together and undergo Rabi oscillations with an effective frequency Ω and damping rate Γ_R. (b) The impurity spectral function of a nearly free impurity (left) is coupled to that of an impurity that strongly interacts with the Fermi gas (right). The repulsive polaron peak is centered at energy E_+ above the molecule-hole continuum and is characterized by the residue Z (dark green area) and width Γ [35].

this branch is important for realizing Fermi gases with strong repulsive interactions [4, 39–43].

In this Letter, we show that the lifetime of the repulsive branch itself is typically much longer than the *quasiparticle lifetime*, which corresponds to the time scale over which the repulsive polaron remains a coherent quasiparticle. The character of the quasiparticle can be probed by driving Rabi oscillations between different internal states of the impurity atom (see Fig. 1), where only one of the states strongly interacts with the surrounding Fermi gas. Previous works have found that the Rabi fre-

quency Ω provides a sensitive probe of the quasiparticle residue Z (squared overlap with the non-interacting impurity state) [7]. Here we demonstrate that the damping rate of oscillations Γ_R is directly linked to the width of the polaron peak in the spectral function, as depicted in Fig. 1(b), which corresponds to the inverse quasiparticle lifetime Γ.

Using a recently developed variational approach [44], we model the Rabi oscillations for two different Fermi-polaron experimental setups: a three-dimensional (3D) ^{6}Li gas with a broad Feshbach resonance [14], and a quasi-two-dimensional (2D) ^{173}Yb gas [16] with an orbital Feshbach resonance [45]. We find that we can capture the Rabi dynamics observed in both experiments, correctly reproducing both Ω and Γ_R even though our approximation neglects relaxation processes to the lower attractive branch at negative energies. We furthermore show that the repulsive polaron in the weak-coupling limit is essentially equivalent to the scenario of a discrete state coupled to a continuum, which differs from the usual Fermi-liquid scenario. Thus, we conclude that the quasiparticle lifetime of the repulsive Fermi polaron in two and three dimensions is primarily limited by many-body dephasing within the upper repulsive branch while relaxation to the attractive branch is negligible, in contrast to the prevailing wisdom (see, e.g., Ref. [4] for a review).

Model.— To model the impurity dynamics in the 3D ^{6}Li experiment of Ref. [14] and the 2D ^{173}Yb experiment of Ref. [16], we use a unified notation where the dimensionality of momenta and sums are implicit. For clarity, even though we consider homonuclear systems, we introduce majority fermion creation operators $\hat{f}_{\mathbf{k}}^\dagger$ and impurity creation operators $\hat{c}_{\mathbf{k},\sigma}^\dagger$ with two different pseudo-spins $\sigma = \uparrow, \downarrow$ (Fig. 1). For a description of the precise relationship to atomic states in experiments, see the Supplemental Material [46].

The Hamiltonian we consider consists of four terms:

$$\hat{H} = \hat{H}_0 + \hat{H}_\uparrow + \hat{H}_\downarrow + \hat{H}_\Omega. \tag{1}$$

The term $\hat{H}_0 = \sum_{\mathbf{k}}(\epsilon_{\mathbf{k}} - \mu)\hat{f}_{\mathbf{k}}^\dagger \hat{f}_{\mathbf{k}}$ describes the medium in the absence of the impurity. Here, $\mathbf{k}$ is the particle momentum, $\epsilon_{\mathbf{k}} = |\mathbf{k}|^2/2m \equiv k^2/2m$ is the kinetic energy, and m is the mass of both the fermions and the impurity (we work in units where $\hbar$ and the system volume or area are set to 1). We use a grand canonical formulation for the medium, with μ the corresponding chemical potential [47, 48].

The impurity spin-σ terms

$$\hat{H}_\sigma = \sum_{\mathbf{k}} \left[\epsilon_{\mathbf{k}} \hat{c}_{\mathbf{k}\sigma}^\dagger \hat{c}_{\mathbf{k}\sigma} + (\epsilon_{\mathbf{k}}/2 + \nu_\sigma)\hat{d}_{\mathbf{k}\sigma}^\dagger \hat{d}_{\mathbf{k}\sigma} \right] \\ + g_\sigma \sum_{\mathbf{k},\mathbf{q}} \left(\hat{d}_{\mathbf{q}\sigma}^\dagger \hat{c}_{\mathbf{q}-\mathbf{k}\sigma} \hat{f}_{\mathbf{k}} + \hat{f}_{\mathbf{k}}^\dagger \hat{c}_{\mathbf{q}-\mathbf{k}\sigma}^\dagger \hat{d}_{\mathbf{q}\sigma} \right), \tag{2}$$

describe the interaction of the impurity and majority fermions via the coupling into a closed channel with creation operator $\hat{d}_{\mathbf{k}\sigma}^\dagger$, where we have coupling constant g_σ and closed-channel detuning ν_σ. Renormalizing the model enables us to trade the bare parameters of the model — the detuning, the coupling constant, and an ultraviolet momentum cutoff — for the physical interaction parameters which parameterize the 2D and 3D impurity-majority fermion low-energy scattering amplitudes

$$f_{2\mathrm{D}\sigma}(k) \simeq \frac{4\pi}{-\ln(k^2 a_{2\mathrm{D}\sigma}^2) + R_{2\mathrm{D}\sigma}^2 k^2 + i\pi}, \tag{3a}$$

$$f_{3\mathrm{D}\sigma}(k) \simeq \frac{1}{-a_{3\mathrm{D}\sigma}^{-1} + ik}, \tag{3b}$$

namely the 2D and 3D scattering lengths, $a_{2\mathrm{D}\sigma}$ and $a_{3\mathrm{D}\sigma}$, and a 2D range parameter $R_{2\mathrm{D}\sigma}$ [46, 49]. The presence of $R_{2\mathrm{D}\sigma}$ in Eq. (3a) allows us to model the strongly energy-dependent scattering close to the ^{173}Yb orbital Feshbach resonance [45, 50, 51] in a 2D geometry. Conversely, we can safely neglect effective range corrections for the broad resonance, 3D case of ^{6}Li. In what follows, we take the impurity spin-$\uparrow$ (spin-$\downarrow$) state to be strongly (weakly) interacting with the medium [46], as depicted in Fig. 1. To simplify notation, we therefore identify $a_{3\mathrm{D}} \equiv a_{3\mathrm{D}\uparrow}$, $a_{2\mathrm{D}} \equiv a_{2\mathrm{D}\uparrow}$, and $R_{2\mathrm{D}} \equiv R_{2\mathrm{D}\uparrow}$.

The radio-frequency [14] or optical [16] fields that couple the impurities in states $\uparrow$ and $\downarrow$ are described within the rotating wave approximation:

$$\hat{H}_\Omega = \frac{\Omega_0}{2} \sum_{\mathbf{k}} \left(\hat{c}_{\mathbf{k}\downarrow}^\dagger \hat{c}_{\mathbf{k}\uparrow} + \hat{c}_{\mathbf{k}\uparrow}^\dagger \hat{c}_{\mathbf{k}\downarrow} \right) + \Delta\omega\, \hat{n}_\downarrow. \tag{4}$$

Here, $\hat{n}_\sigma = \sum_{\mathbf{k}} \left(\hat{c}_{\mathbf{k}\sigma}^\dagger \hat{c}_{\mathbf{k}\sigma} + \hat{d}_{\mathbf{k}\sigma}^\dagger \hat{d}_{\mathbf{k}\sigma} \right)$ is the spin-σ impurity number operator, Ω_0 is the (bare) Rabi coupling, and $\Delta\omega$ is the detuning from the bare $\downarrow$-$\uparrow$ transition.

Perturbative analysis.— We can gain insight into the nature of the repulsive Fermi polaron by analyzing the quasiparticle peak in the spectrum at weak interactions and temperature $T = 0$, such that the polaron is at rest. Focussing on the 3D case, in the limit $k_F a_{3D} \ll 1$ the polaron energy E_+ is given by the mean-field expression $E_+ = \frac{4k_F a_{3\mathrm{D}}}{3\pi} E_F + O(a_{3\mathrm{D}}^2)$ [52], where $E_F = \frac{k_F^2}{2m}$ is the Fermi energy with k_F the Fermi momentum. Thus, the quasiparticle state is pushed up into the continuum of scattering states that exists above zero energy in the case of attractive interactions. In particular, by performing a perturbative analysis [46], we find that the broadening of the quasiparticle peak [Fig. 1(b)] is dominated by the coupling to this continuum, such that the leading order behavior is

$$\Gamma \simeq \frac{8(k_F a_{3\mathrm{D}})^4}{9\pi^3} E_F \simeq 0.029\,(k_F a_{3\mathrm{D}})^4 E_F. \tag{5}$$

This has two important consequences. First, at orders below $a_{3\mathrm{D}}^4$, the quasiparticle behavior is indistinguishable from the case of truly repulsive interactions, where
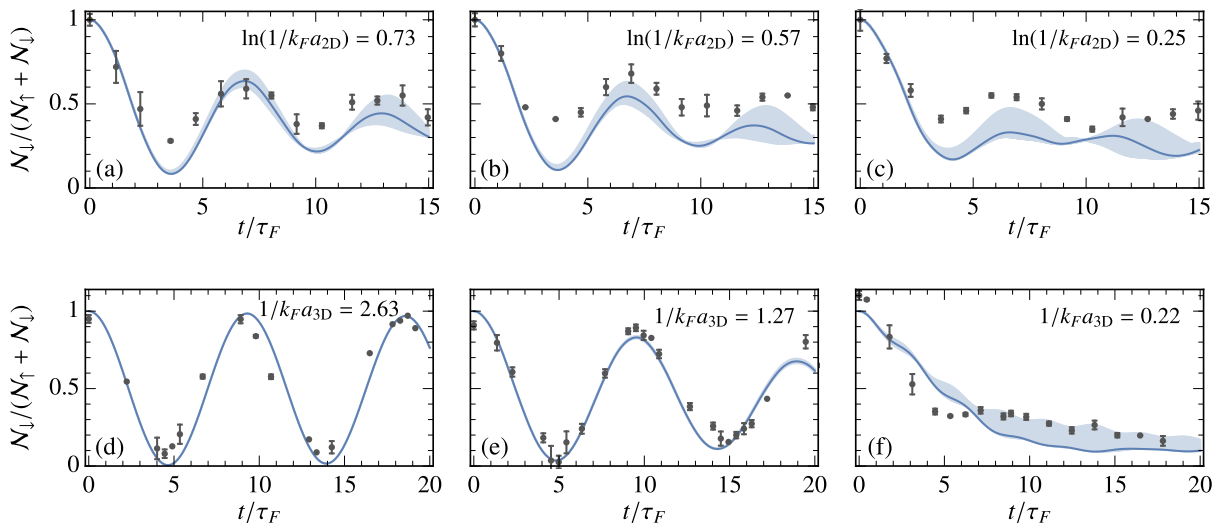
FIG. 2. Rabi oscillations calculated using the TBM (solid lines) and compared with the data (black dots) from the 2D ^{173}Yb experiment [16] (top row) and the 3D ^{6}Li experiment [14] (bottom row). In the top row, $\Omega_0/E_F \simeq 0.95$ and $T/T_F \simeq 0.16$ while, from left to right, $\ln(1/k_F a_{2D}) = 0.73$, 0.57, and 0.25. In the bottom row, $\Omega_0/E_F \simeq 0.68$ and $T/T_F \simeq 0.13$ while, from left to right, $1/(k_F a) = 2.63$, 1.27, and 0.22. The shaded regions correspond to the estimated uncertainty in the detuning around the repulsive polaron energy [46]. In the top row, the data is calculated from the sole measurement of $\mathcal{N}_\downarrow(t)$, and the normalization of each data point to $\mathcal{N}_\downarrow(t=0)$ [46]. We define the Fermi time $\tau_F \equiv 1/E_F$.

the lifetime would be infinite [34, 52]. In this regime, the repulsive polaron is adiabatically connected to the non-interacting impurity. Second, the contribution to the quasiparticle width from relaxation to the attractive branch is negligible in this limit, since it is dominated by three-body recombination [14] and takes the form $\Gamma_3 \simeq 0.025(k_F a_{3D})^6 E_F \ll \Gamma$ [53]. This illustrates that — within the perturbative regime — the finite quasiparticle lifetime arises from many-body dephasing processes that are manifestly distinct from relaxation to negative-energy states. Moreover, this cannot be viewed as momentum relaxation like in usual Fermi liquid theory [1], since we are considering a *zero-momentum* quasiparticle.

Rabi oscillations as a probe of quasiparticles.— We now argue that Rabi oscillations provide a sensitive probe of the repulsive polaron width (or quasiparticle lifetime). We focus on zero total momentum, since we are interested in decoherence effects beyond the standard momentum relaxation occurring in Fermi liquid theory [1]. At times $t \geq 0$, the impurity population in spin σ is

$$\mathcal{N}_\sigma(t) = \text{Tr}[\hat{\rho}_0 \hat{c}(t) \hat{n}_\sigma \hat{c}^\dagger(t)], \qquad (6)$$

where $\hat{c}(t)$ is the impurity operator in the Heisenberg picture. Here, our initial state $\hat{c}(t=0) = \hat{c}_{\mathbf{0}\downarrow}$ is chosen such that $\mathcal{N}_\downarrow(0) = 1$ and $\mathcal{N}_\uparrow(0) = 0$. The trace is over all states of the medium in the absence of the impurity, and we use the thermal density matrix $\hat{\rho}_0 = \exp(-\beta \hat{H}_0)/\text{Tr}[\exp(-\beta \hat{H}_0)]$ with $\beta \equiv 1/T$ (we set the Boltzmann constant to 1). Under the assumption that $\hat{n}_\downarrow \simeq \hat{c}_{\mathbf{0}\downarrow}^\dagger \hat{c}_{\mathbf{0}\downarrow}$ (which would be true for impurities with

infinite mass), we find [46]

$$\mathcal{N}_\downarrow(t) \simeq \int d\omega d\omega' \, \tilde{A}_\downarrow(\omega) \tilde{A}_\downarrow(\omega') e^{-i(\omega-\omega')t}, \qquad (7)$$

where $\tilde{A}_\downarrow(\omega)$ is the spin-↓ impurity spectral function in the presence of Rabi coupling. Taking the Rabi oscillations to be on resonance with the repulsive quasiparticle, i.e., $\Delta\omega = E_+$, we can furthermore approximate the spin-dependent impurity Green's functions in the absence of Rabi coupling as $G_\downarrow(\omega) \simeq 1/(\omega - E_+ + i\eta)$ and $G_\uparrow(\omega) \simeq Z/(\omega - E_+ + i\Gamma)$, where Z is the quasiparticle residue and η is a convergence factor that implicitly carries the limit $\eta \to 0^+$. With these approximations and as long as $\Gamma \lesssim \sqrt{Z}\Omega_0$, we finally obtain [46]

$$\mathcal{N}_\downarrow(t) \simeq e^{-\Gamma t} \left[\frac{1}{2} + \frac{1}{2}\cos\left(t\sqrt{\Omega_0^2 Z - \Gamma^2}\right) \right]. \qquad (8)$$

Equation (8) provides two valuable insights. First, the Rabi oscillation frequency Ω is related to the residue via $Z \simeq (\Omega^2 + \Gamma^2)/\Omega_0^2$, which provides a correction to the standard approximation of $Z \simeq (\Omega/\Omega_0)^2$ [7]. Second, we see that the damping of Rabi oscillations is precisely the quasiparticle width Γ. This key result has been observed in experiment [14, 16] but has previously lacked theoretical support.

Variational approach.— We now turn to modelling the experimental Rabi oscillations. We apply the finite-temperature variational approach developed in Ref. [44] in the context of Ramsey spectroscopy of impurities in a Fermi sea [13] (see also Ref. [54] for a related zero-temperature approach). The idea in this truncated basis

method (TBM) is to introduce a time-dependent variational impurity operator $\hat{c}(t) = \hat{c}_\uparrow(t) + \hat{c}_\downarrow(t)$ that only approximately satisfies the Heisenberg equation of motion. This allows us to introduce an error operator $\hat{\epsilon}(t) \equiv i\partial_t \hat{c}(t) - [\hat{c}(t), \hat{H}]$ and an associated error quantity $\Delta(t) \equiv \text{Tr}\big[\hat{\rho}_0 \hat{\epsilon}(t)\hat{\epsilon}^\dagger(t)\big]$. Our variational ansatz for the spin-σ component of the impurity operator is inspired by the work of Chevy [24] and corresponds to

$$\hat{c}_\sigma(t) = \alpha_0^\sigma(t)\hat{c}_{\mathbf{0}\sigma} + \sum_{\mathbf{k}} \alpha_{\mathbf{k}}^\sigma(t)\hat{f}_{\mathbf{k}}^\dagger \hat{d}_{\mathbf{k}\sigma} + \sum_{\mathbf{k},\mathbf{q}} \alpha_{\mathbf{k}\mathbf{q}}^\sigma(t)\hat{f}_{\mathbf{q}}^\dagger \hat{f}_{\mathbf{k}} \hat{c}_{\mathbf{q}-\mathbf{k}\sigma}. \tag{9}$$

The variational operator consists of three terms: the bare impurity, the impurity bound to a fermion in a closed-channel dimer, and the impurity with a particle-hole excitation. The time dependence is entirely contained within the variational coefficients $\{\alpha\}$, allowing us to impose the minimization condition $\partial\Delta(t)/\partial\dot{\alpha}_j^{\sigma*}(t) = 0$. Since the Rabi coupling is suddenly turned on at $t = 0$, we can use the stationary solutions obtained from a set of linear equations for the expansion coefficients. This follows Ref. [44] with straightforward modifications due to the two possible impurity spin states [46].

Following the application of an external driving field, we obtain the Rabi oscillations within our variational approach via Eq. (6). We show the resulting Rabi oscillations in Fig. 2 for a representative set of interaction strengths and temperatures T/T_F in both two and three dimensions, where the Fermi temperature $T_F = E_F$. Here we set the detuning to match the theoretical repulsive polaron energy, with a small shift due to initial state interactions [46]. The shaded regions illustrate the range of possible results that can be obtained by varying the detuning within the width of the repulsive polaron quasiparticle peak [46]. This accounts for the Rabi oscillations being slightly off resonance in experiment due to the non-zero density of impurities, the density inhomogeneity within the trap, and other technical limitations.

Figure 2 demonstrates that our variational approach captures the Rabi oscillations between the bare impurity and the repulsive polaron in the 2D [16] and 3D [14] experiments. We note that there is a small positive offset in the 2D data [46], which does not strongly affect the extracted Rabi parameters. Crucially, our variational ansatz does not incorporate any processes where the repulsive polaron decays into the attractive branch, because these involve additional particle-hole excitations [35] which are neglected in Eq. (9). Therefore, the consistency between our theoretical results and the experiments provides strong evidence that the decoherence in the Rabi oscillations — and hence the inverse quasiparticle lifetime Γ — is physically dominated by the coupling to the continuum at positive energies, rather than by relaxation to the attractive branch. Given the fundamental differences between the two experiments [14, 16],
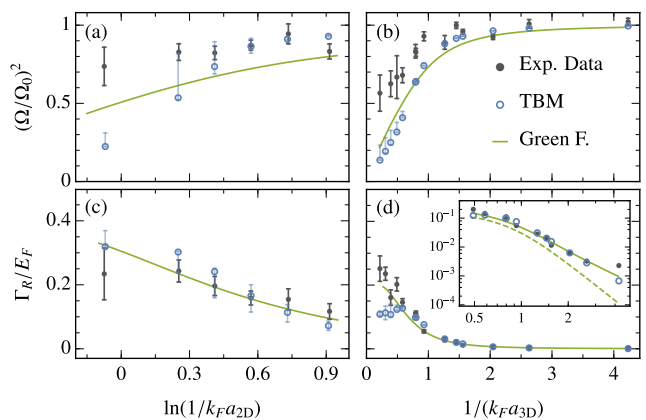

FIG. 3. The extracted frequency $(\Omega/\Omega_0)^2$ and damping Γ_R of the Rabi oscillations as determined from the TBM (blue circles) and in the 2D (a,c) and 3D (b,d) experiments (black dots). The TBM error bars are derived from the uncertainty in detuning [46], which tends to increase the oscillation frequency. The extracted Rabi parameters are also compared with the quasiparticle residue $Z \simeq (\Omega/\Omega_0)^2$ (top row) and quasiparticle inverse lifetime $\Gamma \simeq \Gamma_R$ (bottom row) obtained directly from the finite-temperature impurity Green's function (green solid line). The TBM simulations are set to match the experimental parameters [46]. Inset: Data in (d) plotted on a log-log scale, together with the result of a zero-temperature Green's function calculation (green dashed line).

we expect this to be a generic feature of the mobile Fermi polaron with short-range attractive interactions.

Quasiparticle properties.— We can further quantify the nature of the repulsive polaron by determining the frequency Ω and damping Γ_R of the observed Rabi oscillations, which can be modelled approximately as [14]:

$$\mathcal{N}_\downarrow(t) \simeq be^{-\Gamma_{\text{bg}}t} + (1-b)e^{-\Gamma_R t}\cos(\Omega t). \tag{10}$$

Here, b is a dimensionless fitting parameter, while Γ_{bg} can be regarded as a background decay rate of the spin-$\downarrow$ state. We see that Eq. (10) reduces to our theoretical expression in Eq. (8) if we set $b = 1/2$ and $\Gamma_{\text{bg}} = \Gamma_R$. In practice, we find that $\Gamma_{\text{bg}} < \Gamma_R$ since there are scattering processes that can populate the spin-$\downarrow$ state without contributing to the damping of oscillations, and these are neglected in our approximation (7) .

Using the fit provided in Eq. (10), we extract both Ω and Γ_R from our simulated Rabi oscillations within the TBM and compare them with the experimental results, as depicted in Fig. 3. We also show the repulsive polaron residue Z and inverse quasiparticle lifetime Γ obtained directly from the impurity Green's function $G_\downarrow(\omega)$, where the impurity self energy is calculated using ladder diagrams [46]. Such an approach is equivalent to our spin-$\downarrow$ variational ansatz in Eq. (9) in the absence of Rabi coupling [44], and similarly it does not include the contribution to the quasiparticle lifetime due to relaxation from the repulsive branch to lower lying states.

Referring to Fig. 3, we see that all three methods are in good agreement with each other for weak to intermediate interaction strengths. This is particularly evident for Γ_R in Fig. 3(d), where the agreement spans two orders of magnitude. Here we find that the finite temperature of the Fermi gas leads to deviations from the perturbative result in Eq. (5), but the behavior is still markedly different from the momentum relaxation predicted by Fermi liquid theory [11]. The observed agreement suggests that temperature predominantly affects the many-body dephasing via thermal fluctuations of the medium rather than through finite impurity momenta. In Fig. 3(a), the slightly elevated values of $(\Omega/\Omega_0)^2$ compared to the expected residue Z can be attributed to the strong Rabi driving $(\Omega_0/E_F \gtrsim 1)$, such that the oscillation period approaches the formation time of the polaron.

At stronger repulsive interactions, there are more pronounced deviations as the repulsive polaron quasiparticle becomes less well defined and the effects of a finite impurity density in experiments are expected to be more important [14]. In particular, it becomes increasingly difficult to extract quasiparticle properties from the Rabi oscillations once the quasiparticle width Γ is comparable to Ω, which is consistent with our theoretical analysis in Eq. (8). This accounts for the suppression of coherent oscillations in Fig. 2(f) as well as the anomalously low Γ_R obtained from the TBM near unitarity in Fig. 3(d). Our results suggest that one could better probe the repulsive polaron quasiparticle lifetime at strong coupling by increasing the Rabi drive Ω_0.

Conclusions.— We have investigated the nature of the repulsive Fermi polaron in two and three dimensions. We have shown that both the quasiparticle lifetime and the residue can be probed by driving Rabi oscillations between weakly and strongly interacting impurity spin states. By simulating the Rabi oscillations in two fundamentally different experiments and by performing a perturbative analysis of the weak-coupling limit, we have demonstrated that the quasiparticle lifetime is determined by many-body dephasing within the upper repulsive branch and is thus typically much shorter than the lifetime of the repulsive branch itself. Our work provides an important benchmark for many-body numerical approaches [55] and it opens up the prospect of exploring a long-lived repulsive Fermi gas with novel excitations beyond the Fermi liquid paradigm.

[1] D. Pines and P. Nozières, *The Theory of Quantum Liquids* (W. A. Benjamin, New York, 1966).

[2] C. Varma, Z. Nussinov, and W. van Saarloos, *Singular or non-Fermi liquids*, Physics Reports **361**, 267 (2002).

[3] M. R. Norman, *The Challenge of Unconventional Superconductivity*, Science **332**, 196 (2011).

[4] P. Massignan, M. Zaccanti, and G. M. Bruun, *Polarons, dressed molecules and itinerant ferromagnetism in ultracold Fermi gases*, Rep. Prog. Phys. **77**, 034401 (2014).

[5] A. Schirotzek, C.-H. Wu, A. Sommer, and M. W. Zwierlein, *Observation of Fermi Polarons in a Tunable Fermi Liquid of Ultracold Atoms*, Phys. Rev. Lett. **102**, 230402 (2009).

[6] S. Nascimbène, N. Navon, K. J. Jiang, L. Tarruell, M. Teichmann, J. McKeever, F. Chevy, and C. Salomon, *Collective Oscillations of an Imbalanced Fermi Gas: Axial Compression Modes and Polaron Effective Mass*, Phys. Rev. Lett. **103**, 170402 (2009).

[7] C. Kohstall, M. Zaccanti, M. Jag, A. Trenkwalder, P. Massignan, G. Bruun, F. Schreck, and R. Grimm, *Metastability and coherence of repulsive polarons in a strongly interacting Fermi mixture*, Nature **485**, 615 (2012).

[8] M. Koschorreck, D. Pertot, E. Vogt, B. Fröhlich, M. Feld, and M. Köhl, *Attractive and repulsive Fermi polarons in two dimensions*, Nature **485**, 619 (2012).

[9] Y. Zhang, W. Ong, I. Arakelyan, and J. E. Thomas, *Polaron-to-Polaron Transitions in the Radio-Frequency Spectrum of a Quasi-Two-Dimensional Fermi Gas*, Phys. Rev. Lett. **108**, 235302 (2012).

[10] A. N. Wenz, G. Zürn, S. Murmann, I. Brouzos, T. Lompe, and S. Jochim, *From Few to Many: Observing the Formation of a Fermi Sea One Atom at a Time*, Science **342**, 457 (2013).

[11] M. Cetina, M. Jag, R. S. Lous, J. T. M. Walraven, R. Grimm, R. S. Christensen, and G. M. Bruun, *Decoherence of Impurities in a Fermi Sea of Ultracold Atoms*, Phys. Rev. Lett. **115**, 135302 (2015).

[12] W. Ong, C. Cheng, I. Arakelyan, and J. E. Thomas, *Spin-Imbalanced Quasi-Two-Dimensional Fermi Gases*, Phys. Rev. Lett. **114**, 110403 (2015).

[13] M. Cetina, M. Jag, R. S. Lous, I. Fritsche, J. T. M. Walraven, R. Grimm, J. Levinsen, M. M. Parish, R. Schmidt, M. Knap, and E. Demler, *Ultrafast many-body interferometry of impurities coupled to a Fermi sea*, Science **354**, 96 (2016).

[14] F. Scazza, G. Valtolina, P. Massignan, A. Recati, A. Amico, A. Burchianti, C. Fort, M. Inguscio, M. Zaccanti, and G. Roati, *Repulsive Fermi Polarons in a Resonant Mixture of Ultracold 6-Li Atoms*, Phys. Rev. Lett. **118**, 083602 (2017).

[15] Z. Yan, P. B. Patel, B. Mukherjee, R. J. Fletcher, J. Struck, and M. W. Zwierlein, *Boiling a Unitary Fermi Liquid*, Phys. Rev. Lett. **122**, 093401 (2019).

[16] N. Darkwah Oppong, L. Riegger, O. Bettermann,

M. Höfer, J. Levinsen, M. M. Parish, I. Bloch, and S. Fölling, *Observation of Coherent Multiorbital Polarons in a Two-Dimensional Fermi Gas*, Phys. Rev. Lett. **122**, 193604 (2019).

[17] G. Ness, C. Shkedrov, Y. Florshaim, and Y. Sagi, *Observation of a smooth polaron-molecule transition in a degenerate Fermi gas*, arXiv e-prints , arXiv:2001.10450 (2020), arXiv:2001.10450 [cond-mat.quant-gas].

[18] J. Catani, G. Lamporesi, D. Naik, M. Gring, M. Inguscio, F. Minardi, A. Kantian, and T. Giamarchi, *Quantum dynamics of impurities in a one-dimensional Bose gas*, Phys. Rev. A **85**, 023623 (2012).

[19] M.-G. Hu, M. J. de Graaff, D. Kedar, J. P. Corson, E. A. Cornell, and D. S. Jin, *Bose Polarons in the Strongly Interacting Regime*, Phys. Rev. Lett. **117**, 055301 (2016).

[20] N. B. Jørgensen, L. Wacker, K. T. Skalmstang, M. M. Parish, J. Levinsen, R. S. Christensen, G. M. Bruun, and J. J. Arlt, *Observation of Attractive and Repulsive Polarons in a Bose-Einstein Condensate*, Phys. Rev. Lett. **117**, 055302 (2016).

[21] F. Camargo, R. Schmidt, J. D. Whalen, R. Ding, G. Woehl, S. Yoshida, J. Burgdörfer, F. B. Dunning, H. R. Sadeghpour, E. Demler, and T. C. Killian, *Creation of Rydberg Polarons in a Bose Gas*, Phys. Rev. Lett. **120**, 083401 (2018).

[22] Z. Z. Yan, Y. Ni, C. Robens, and M. W. Zwierlein, *Bose polarons near quantum criticality*, Science **368**, 190 (2020).

[23] M. Sidler, P. Back, O. Cotlet, A. Srivastava, T. Fink, M. Kroner, E. Demler, and A. Imamoglu, *Fermi polaron-polaritons in charge-tunable atomically thin semiconductors*, Nat. Phys. **13**, 255 (2017).

[24] F. Chevy, *Universal phase diagram of a strongly interacting Fermi gas with unbalanced spin populations*, Phys. Rev. A **74**, 063628 (2006).

[25] R. Combescot, A. Recati, C. Lobo, and F. Chevy, *Normal State of Highly Polarized Fermi Gases: Simple Many-Body Approaches*, Phys. Rev. Lett. **98**, 180402 (2007).

[26] N. Prokof'ev and B. Svistunov, *Fermi-polaron problem: Diagrammatic Monte Carlo method for divergent sign-alternating series*, Phys. Rev. B **77**, 020408 (2008).

[27] R. Combescot and S. Giraud, *Normal state of highly polarized fermi gases: Full many-body treatment*, Phys. Rev. Lett. **101**, 050404 (2008).

[28] M. Punk, P. T. Dumitrescu, and W. Zwerger, *Polaron-to-molecule transition in a strongly imbalanced Fermi gas*, Phys. Rev. A **80**, 053605 (2009).

[29] C. J. M. Mathy, M. M. Parish, and D. A. Huse, *Trimers, Molecules, and Polarons in Mass-Imbalanced Atomic Fermi Gases*, Phys. Rev. Lett. **106**, 166404 (2011).

[30] R. Schmidt and T. Enss, *Excitation spectra and rf response near the polaron-to-molecule transition from the functional renormalization group*, Phys. Rev. A **83**, 063620 (2011).

[31] C. Trefzger and Y. Castin, *Impurity in a Fermi sea on a narrow Feshbach resonance: A variational study of the polaronic and dimeronic branches*, Phys. Rev. A **85**, 053612 (2012).

[32] J. Levinsen and M. M. Parish, *Strongly interacting two-dimensional Fermi gases*, Annu. Rev. Cold Atoms Mol. **3**, 1 (2015).

[33] X. Cui and H. Zhai, *Stability of a fully magnetized ferromagnetic state in repulsively interacting ultracold Fermi gases*, Phys. Rev. A **81**, 041602 (2010).

[34] S. Pilati, G. Bertaina, S. Giorgini, and M. Troyer, *Itinerant Ferromagnetism of a Repulsive Atomic Fermi Gas: A Quantum Monte Carlo Study*, Phys. Rev. Lett. **105**, 030405 (2010).

[35] P. Massignan and G. M. Bruun, *Repulsive polarons and itinerant ferromagnetism in strongly polarized Fermi gases*, Eur. Phys. J. D **65**, 83 (2011).

[36] O. Goulko, A. S. Mishchenko, N. Prokof'ev, and B. Svistunov, *Dark continuum in the spectral function of the resonant Fermi polaron*, Phys. Rev. A **94**, 051605 (2016).

[37] H. Tajima and S. Uchino, *Many Fermi polarons at nonzero temperature*, New J. Phys. **20**, 073048 (2018).

[38] B. C. Mulkerin, X.-J. Liu, and H. Hu, *Breakdown of the Fermi polaron description near Fermi degeneracy at unitarity*, Ann. Phys. (N. Y.) **407**, 29 (2019).

[39] D. Pekker, M. Babadi, R. Sensarma, N. Zinner, L. Pollet, M. W. Zwierlein, and E. Demler, *Competition between Pairing and Ferromagnetic Instabilities in Ultracold Fermi Gases near Feshbach Resonances*, Phys. Rev. Lett. **106**, 050402 (2011).

[40] C. Sanner, E. J. Su, W. Huang, A. Keshet, J. Gillen, and W. Ketterle, *Correlations and Pair Formation in a Repulsively Interacting Fermi Gas*, Phys. Rev. Lett. **108**, 240404 (2012).

[41] G. Valtolina, F. Scazza, A. Amico, A. Burchianti, A. Recati, T. Enss, M. Inguscio, M. Zaccanti, and G. Roati, *Exploring the ferromagnetic behaviour of a repulsive Fermi gas through spin dynamics*, Nature Phys. **13**, 704 (2017).

[42] A. Amico, F. Scazza, G. Valtolina, P. E. S. Tavares, W. Ketterle, M. Inguscio, G. Roati, and M. Zaccanti, *Time-Resolved Observation of Competing Attractive and Repulsive Short-Range Correlations in Strongly Interacting Fermi Gases*, Phys. Rev. Lett. **121**, 253602 (2018).

[43] F. Scazza, G. Valtolina, A. Amico, P. E. S. Tavares, M. Inguscio, W. Ketterle, G. Roati, and M. Zaccanti, *Exploring emergent heterogeneous phases in strongly repulsive Fermi gases*, Phys. Rev. A **101**, 013603 (2020).

[44] W. E. Liu, J. Levinsen, and M. M. Parish, *Variational Approach for Impurity Dynamics at Finite Temperature*, Phys. Rev. Lett. **122**, 205301 (2019).

[45] R. Zhang, Y. Cheng, H. Zhai, and P. Zhang, *Orbital Feshbach Resonance in Alkali-Earth Atoms*, Phys. Rev. Lett. **115**, 135301 (2015).

[46] See the supplemental material for details of the model and scattering parameters, the variational approach, the perturbative analysis, and the relationship between Rabi oscillations and the quasiparticle width. This includes a table of experimental parameters used for the TBM simulations, as well as Refs. [56–60].

[47] W. E. Liu, Z.-Y. Shi, J. Levinsen, and M. M. Parish, *Radio-frequency response and contact of impurities in a quantum gas* (2020), arXiv:2002.01224 [cond-mat.quant-gas].

[48] W. E. Liu, Z.-Y. Shi, M. M. Parish, and J. Levinsen, *Theory of radio-frequency spectroscopy of impurities in quantum gases* (2020), arXiv:2002.01211 [cond-mat.quant-gas].

[49] J. Levinsen and M. M. Parish, *Bound States in a Quasi-Two-Dimensional Fermi Gas*, Phys. Rev. Lett. **110**, 055304 (2013).

[50] M. Höfer, L. Riegger, F. Scazza, C. Hofrichter, D. R. Fernandes, M. M. Parish, J. Levinsen, I. Bloch, and

S. Fölling, *Observation of an Orbital Interaction-Induced Feshbach Resonance in* ^{173}Yb, Phys. Rev. Lett. **115**, 265302 (2015).

[51] G. Pagano, M. Mancini, G. Cappellini, L. Livi, C. Sias, J. Catani, M. Inguscio, and L. Fallani, *Strongly Interacting Gas of Two-Electron Fermions at an Orbital Feshbach Resonance*, Phys. Rev. Lett. **115**, 265301 (2015).

[52] R. Bishop, *On the ground state of an impurity in a dilute fermi gas*, Ann. Phys. (N. Y.) **78**, 391 (1973).

[53] D. S. Petrov, *Three-body problem in Fermi gases with short-range interparticle interaction*, Phys. Rev. A **67**, 010703 (2003).

[54] M. M. Parish and J. Levinsen, *Quantum dynamics of impurities coupled to a Fermi sea*, Phys. Rev. B **94**, 184303 (2016).

[55] O. Goulko, A. S. Mishchenko, L. Pollet, N. Prokof'ev, and B. Svistunov, *Numerical analytic continuation: Answers to well-posed questions*, Phys. Rev. B **95**, 014102 (2017).

[56] J. Xu, R. Zhang, Y. Cheng, P. Zhang, R. Qi, and H. Zhai, *Reaching a Fermi-superfluid state near an orbital Feshbach resonance*, Phys. Rev. A **94**, 033609 (2016).

[57] T. Kirk and M. M. Parish, *Three-body correlations in a two-dimensional SU(3) Fermi gas*, Phys. Rev. A **96**, 053614 (2017).

[58] V. Gurarie and L. Radzihovsky, *Resonantly paired fermionic superfluids*, Ann. Phys. (N. Y.) **322**, 2 (2007).

[59] D. S. Petrov and G. V. Shlyapnikov, *Interatomic collisions in a tightly confined Bose gas*, Phys. Rev. A **64**, 012706 (2001).

[60] I. Bloch, J. Dalibard, and W. Zwerger, *Many-body physics with ultracold gases*, Rev. Mod. Phys. **80**, 885 (2008).

SUPPLEMENTAL MATERIAL:
"QUASIPARTICLE LIFETIME OF THE REPULSIVE FERMI POLARON"

Haydn S. Adlong,[1] Weizhe Edward Liu,[1,2] Francesco Scazza,[3] Matteo Zaccanti,[3] Nelson Darkwah Oppong,[4,5,6]
Simon Fölling,[4,5,6] Meera M. Parish,[1,2] and Jesper Levinsen[1,2],

[1]*School of Physics and Astronomy, Monash University, Victoria 3800, Australia*
[2]*ARC Centre of Excellence in Future Low-Energy Electronics Technologies, Monash University, Victoria 3800, Australia*
[3]*Istituto Nazionale di Ottica del Consiglio Nazionale delle Ricerche (CNR-INO) and European Laboratory for Nonlinear
Spectroscopy (LENS), 50019 Sesto Fiorentino, Italy*
[4]*Ludwig-Maximilians-Universität, Schellingstraße 4, 80799 München, Germany*
[5]*Max-Planck-Institut für Quantenoptik, Hans-Kopfermann-Straße 1, 85748 Garching, Germany*
[6]*Munich Center for Quantum Science and Technology (MCQST), Schellingstraße 4, 80799 München, Germany*

MODEL AND SCATTERING PARAMETERS

Model

In modelling the dynamics of impurities coupled to a Fermi sea, we use the following effective Hamiltonian

$$\hat{H} = \hat{H}_0 + \hat{H}_\Omega + \hat{H}_\uparrow + \hat{H}_\downarrow, \tag{S1}$$

where

$$\hat{H}_0 = \sum_{\mathbf{k}} (\epsilon_{\mathbf{k}} - \mu) \hat{f}_{\mathbf{k}}^\dagger \hat{f}_{\mathbf{k}}, \tag{S2a}$$

$$\hat{H}_\Omega = \frac{\Omega_0}{2} \sum_{\mathbf{k}} \left(\hat{c}_{\mathbf{k}\downarrow}^\dagger \hat{c}_{\mathbf{k}\uparrow} + \hat{c}_{\mathbf{k}\uparrow}^\dagger \hat{c}_{\mathbf{k}\downarrow} \right) + \Delta\omega \, \hat{n}_\downarrow, \tag{S2b}$$

$$\hat{H}_\sigma = \sum_{\mathbf{k}} \left[\epsilon_{\mathbf{k}} \hat{c}_{\mathbf{k}\sigma}^\dagger \hat{c}_{\mathbf{k}\sigma} + (\epsilon_{\mathbf{k}}/2 + \nu_\sigma) \hat{d}_{\mathbf{k}\sigma}^\dagger \hat{d}_{\mathbf{k}\sigma} \right] + g_\sigma \sum_{\mathbf{k},\mathbf{q}} \left(\hat{d}_{\mathbf{q}\sigma}^\dagger \hat{c}_{\mathbf{q}/2-\mathbf{k},\sigma} \hat{f}_{\mathbf{q}/2+\mathbf{k}} + \hat{f}_{\mathbf{q}/2+\mathbf{k}}^\dagger \hat{c}_{\mathbf{q}/2-\mathbf{k},\sigma}^\dagger \hat{d}_{\mathbf{q}\sigma} \right). \tag{S2c}$$

The meaning of the various symbols is discussed in the main text.

Relation between Hamiltonian operators and experimental atomic states

In the 2D ^{173}Yb experiment of Ref. [16], the states of the atoms are defined by the electronic state, with ground state $^1S_0$ and long-lived excited state $^3P_0$ (i.e., the "clock" state), as well as the nuclear-spin state with $m_F \in \{-5/2, -3/2, \ldots, +5/2\}$. The majority $\hat{f}_{\mathbf{k}}^\dagger$ atoms exist in the $m_F = +5/2$ ground state, which acts as a bath for the weakly interacting $\hat{c}_{\mathbf{k}\downarrow}^\dagger$ and resonantly interacting $\hat{c}_{\mathbf{k}\uparrow}^\dagger$ impurities in the $m_F = -3/2$ ground state and $m_F = -5/2$ 'clock' state, respectively. Interactions between the $\hat{c}_{\mathbf{k}\uparrow}^\dagger$ and $\hat{f}_{\mathbf{k}}^\dagger$ atoms are tunable through an orbital Feshbach resonance [45] as has been demonstrated experimentally [50, 51].

On the other hand, the 3D experiment of Ref. [14] involves ^{6}Li atoms in the three lowest Zeeman levels. The majority $\hat{f}_{\mathbf{k}}^\dagger$ atoms exist in the lowest Zeeman level, while the weakly interacting $\hat{c}_{\mathbf{k}\downarrow}^\dagger$ and resonantly interacting $\hat{c}_{\mathbf{k}\uparrow}^\dagger$ impurities occupy the second-lowest and third-lowest Zeeman levels respectively. Owing to two off-centered broad Feshbach resonances, the scattering between the $\hat{c}_{\mathbf{k}\uparrow}^\dagger$ and $\hat{f}_{\mathbf{k}}^\dagger$ atoms can be resonantly enhanced while only moderately increasing the comparatively weak interactions between the $\hat{c}_{\mathbf{k}\downarrow}^\dagger$ and $\hat{f}_{\mathbf{k}}^\dagger$ atoms [14].

Scattering parameters

Within the model in Eq. (S1), fermions of the same spin do not interact and the two spin states of the impurity are only coupled through the light-field. Ignoring for the moment the light-field (i.e., setting $\Omega_0 = 0$), we calculate the vacuum spin-dependent impurity-fermion T matrix, which characterizes the interactions between the majority

fermions and a particular spin state of the impurity. This yields

$$T_\sigma(E) = \left[\frac{E - \nu_\sigma}{g_\sigma^2} - \sum_{\mathbf{k}}^{\Lambda} \frac{1}{E - 2\epsilon_{\mathbf{k}}} \right]^{-1}, \tag{S3}$$

where E is the collision energy and Λ is the ultraviolet cutoff.

To proceed, we compare the scattering T matrix with the 2D and 3D scattering amplitudes using $f_{2D\sigma}(k) = mT_\sigma(E)$ and $f_{3D\sigma}(k) = -\frac{m}{4\pi}T_\sigma(E)$, with $E = k^2/m$. The scattering amplitudes at low energy are known to take the forms

$$f_{2D\sigma}(k) \simeq \frac{4\pi}{-\ln(k^2 a_{2D\sigma}^2) + R_{2D\sigma}^2 k^2 + i\pi}, \tag{S4a}$$

$$f_{3D\sigma}(k) \simeq -\frac{1}{a_{3D\sigma}^{-1} + R_{3D\sigma}k^2 + ik}. \tag{S4b}$$

By comparing Eq. (S3) with the low-energy scattering amplitudes, we obtain the renormalized scattering parameters. In 2D, this results in

$$\frac{\nu_\sigma + E_{2\sigma}}{g_\sigma^2} = \sum_{\mathbf{k}}^{\Lambda} \frac{1}{E_{2\sigma} + 2\epsilon_{\mathbf{k}}}, \qquad R_{2D\sigma}^2 = \frac{4\pi}{m^2 g_\sigma^2}, \tag{S5}$$

where $a_{2D\sigma}$ is the scattering length, $R_{2D\sigma}$ is the effective range [57], and $E_{2\sigma}$ is the binding energy of the two-body bound state that exists for all interactions in 2D:

$$E_{2\sigma} = \frac{1}{mR_{2D\sigma}^2} W\left(\frac{R_{2D\sigma}^2}{a_{2D\sigma}^2} \right), \tag{S6}$$

with W the Lambert W function. In 3D, we have

$$\frac{m}{4\pi a_{3D\sigma}} = -\frac{\nu_\sigma}{g_\sigma^2} + \sum_{\mathbf{k}}^{\Lambda} \frac{1}{2\epsilon_{\mathbf{k}}}, \qquad R_{3D\sigma} = \frac{4\pi}{m^2 g_\sigma^2}, \tag{S7}$$

where $a_{3D\sigma}$ is the scattering length and $R_{3D\sigma}$ is a range parameter [58]. In this case, we only have a bound state when $a_{3D\sigma} > 0$, with corresponding binding energy

$$E_{3\sigma} = \frac{\left[\sqrt{1 + 4R_{3D\sigma}/a_{3D\sigma}} - 1 \right]^2}{4mR_{3D\sigma}^2}. \tag{S8}$$

Through this procedure, we have related the bare interaction parameters g, Λ, and ν to the physical parameters, the scattering length a and effective range R, which characterises the relevant Feshbach resonance. For the broad Feshbach resonances in ^{6}Li we use $R_{3D\sigma} = 0$ for both spin states. For the orbital Feshbach resonance in quasi-2D, the description of the effective range is somewhat more complicated, as discussed in the following.

Effective model for scattering at an orbital Feshbach resonance in the presence of confinement

We now discuss how the scattering parameters, $a_{2D\sigma}$ and $R_{2D\sigma}$, of the ^{173}Yb experiment are determined. The orbital Feshbach resonance is known to lead to a strongly energy dependent scattering [45], which is well approximated by the introduction of a 3D effective range [56]. Furthermore, quasi-2D confinement generally leads to a non-trivial energy dependence of the effective 2D scattering amplitude even for a broad Feshbach resonance [59]; for strong confinement, this energy dependence can be modelled by the introduction of a 2D effective range [49]. Thus, we use the effective range in our model to provide the simplest possible description of both the orbital Feshbach resonance and the confinement. This greatly simplifies the numerical simulations of Rabi oscillations, since it drastically reduces the possible degrees of freedom in the problem.

We now describe the possible scattering channels in ^{173}Yb atoms close to an orbital Feshbach resonance, following the analysis in Ref. [45]. We focus on the two electronic orbitals described above (denoted here by $|g\rangle$ and $|e\rangle$) as well as two particular nuclear spin states (denoted here by $|\Downarrow\rangle$ and $|\Uparrow\rangle$). These states form the open channel
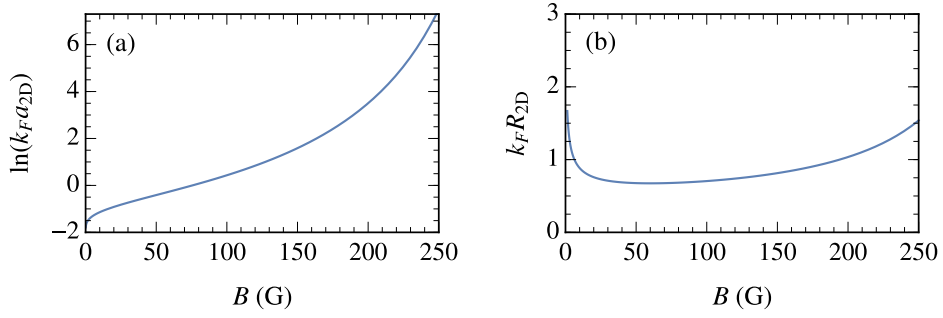
FIG. S1. The open channel 2D scattering length (a) and 2D effective range (b) as a function of magnetic field strength (in Gauss). These parameters are used to create an effective 2D two-channel model description of scattering at an orbital Feshbach resonance in the presence of confinement. To match Ref. [16] we use $\omega_z = 2\pi \times 37.1\,\text{kHz}$.

$|o\rangle \equiv |g \Uparrow, e \Downarrow\rangle$ and the closed channel $|c\rangle \equiv |e \Uparrow, g \Downarrow\rangle$, which are detuned by $\delta = \Delta\mu B$, where $\Delta\mu = h \times 554\,\text{Hz/G}$ [16] is the differential Zeeman shift and B is the magnetic field strength in Gauss. The interactions in this system are not diagonal in the open- and closed-channel basis, but instead proceed via the triplet $(+)$ and singlet $(-)$ channels, with $|\pm\rangle \equiv \frac{1}{\sqrt{2}}(|o\rangle \pm |c\rangle)$. Associated with the singlet and triplet interactions are the singlet and triplet scattering lengths $a_\pm$ [45] and effective ranges $r_\pm$ [50].

In the experiment [16], the ^{173}Yb atoms were confined to move in a 2D plane with a harmonic potential $V(z) = \frac{1}{2}m\omega_z^2 z^2$ acting in the transverse direction. Reference [16] used this to extend the theoretical analysis of quasi-2D scattering in Refs. [59, 60] to derive an effective scattering amplitude of the form in Eq. (S4a). For the weakly interacting $\downarrow$ state, it was found that $\ln(k_F a_{2D\downarrow}) \simeq -4.9(1)$ [16]. In this case, the dependence on $R_{2D\downarrow}$ is strongly suppressed, and we simply take $R_{2D\downarrow} = 0$. For the case of strong interactions, the open channel scattering amplitude was found to be given by [16]

$$f_{q2D}(E) = 2\sqrt{2\pi}\frac{l_z\left(\tilde{a}_-^{-1} - \frac{mr_-E}{2}\right) + l_z\left(\tilde{a}_+^{-1} - \frac{mr_+E}{2}\right) - 2\mathcal{F}\left(\frac{-E+\delta}{\omega_z}\right)}{\left\{\begin{array}{c} -\mathcal{F}\left(\frac{-E+\delta}{\omega_z}\right)\left[l_z(\tilde{a}_-^{-1} - \frac{mr_-E}{2}) + l_z(\tilde{a}_+^{-1} - \frac{mr_+E}{2}) - 2\mathcal{F}\left(-\frac{E}{\omega_z}\right)\right] \\ -\mathcal{F}\left(-\frac{E}{\omega_z}\right)\left[l_z(\tilde{a}_-^{-1} - \frac{mr_-E}{2}) + l_z(\tilde{a}_+^{-1} - \frac{mr_+E}{2})\right] + 2l_z^2(\tilde{a}_-^{-1} - \frac{mr_-E}{2})(\tilde{a}_+^{-1} - \frac{mr_+E}{2}) \end{array}\right\}}, \quad \text{(S9)}$$

where $l_z = 1/\sqrt{m\omega_z}$ and $\tilde{a}_\pm^{-1} = a_\pm^{-1} - \frac{r_\pm}{4l_z^2}(1 - \delta/\omega_z)$. Here, $\mathcal{F}$ is a transcendental function defined by [60]

$$\mathcal{F}(x) = \int_0^\infty \frac{du}{\sqrt{4\pi u^3}}\left[1 - \frac{e^{-xu}}{\sqrt{(1 - e^{-2u})/2u}}\right], \quad \text{(S10)}$$

and the energy is measured with respect to the quasi-2D zero point energy.

To extract an effective low-energy open-channel 2D scattering length and effective range for the strongly interacting spin-$\uparrow$ impurity case, we perform a low energy expansion of Eq. (S9) and compare it with the standard form of the low-energy scattering amplitude, Eq. (S4a). In the following, we use the notation $a_{2D} \equiv a_{2D\uparrow}$ and $R_{2D} \equiv R_{2D\uparrow}$, as in the main text. Assuming that $\delta \gg |E|$ (i.e., that we are not close to $B = 0$) we find the 2D scattering length [16]

$$a_{2D} = l_z\sqrt{\frac{\pi}{D}}\exp\left[-\sqrt{2\pi}\frac{l_z^2(\tilde{a}_- \tilde{a}_+)^{-1} - \frac{1}{2}(l_z\tilde{a}_-^{-1} + l_z\tilde{a}_+^{-1})\mathcal{F}\left(\frac{\delta}{\omega_z}\right)}{l_z\tilde{a}_-^{-1} + l_z\tilde{a}_+^{-1} - 2\mathcal{F}\left(\frac{\delta}{\omega_z}\right)}\right], \quad \text{(S11)}$$

where $D \simeq 0.905$ [59]. The 2D effective range takes the form

$$\left(\frac{R_{2D}}{l_z}\right)^2 = \ln 2 - \frac{\sqrt{2\pi}\left\{l_z^{-1}r_+\left[l_z\tilde{a}_-^{-1} - \mathcal{F}\left(\frac{\delta}{\omega_z}\right)\right]^2 + l_z^{-1}r_-\left[l_z\tilde{a}_+^{-1} - \mathcal{F}\left(\frac{\delta}{\omega_z}\right)\right]^2 + \left[l_z\tilde{a}_-^{-1} - l_z\tilde{a}_+^{-1}\right]^2\mathcal{F}'\left(\frac{\delta}{\omega_z}\right)\right\}}{\left(l_z\tilde{a}_-^{-1} + l_z\tilde{a}_+^{-1} - 2\mathcal{F}\left(\frac{\delta}{\omega_z}\right)\right)^2}, \quad \text{(S12)}$$

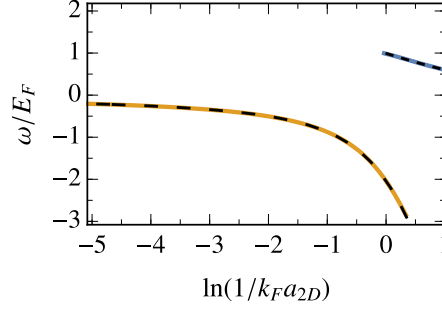where $\mathcal{F}'$ is the first derivative of $\mathcal{F}$.

FIG. S2. The attractive (orange) and repulsive (blue) Fermi polaron energy as calculated through our effective two-channel model description of an orbital Feshbach resonance in the presence of confinement. The energies are highly consistent with the full theory calculation of the polaron energies (black) from Ref. [16]. The curves are calculated at temperature $T/T_F = 0.16$.

Figure S1 shows the extracted scattering parameters using the experimentally determined values for all parameters [16] (see also Ref. [50]). We see that indeed the change of the magnetic field provides a means to tune the interactions via a_{2D}. On the other hand, the effective range is not strongly dependent on magnetic field — indeed, the effective range is approximately constant ($k_F R_{2D} \sim 1$) within the magnetic field strengths of interest to the present work.

In general, we find that the 2D effective range is able to highly accurately capture the physics of the orbital Feshbach resonance and the confinement in the domain of interaction strengths used in Ref. [16]. This is shown in Fig. S2, where we show the near perfect agreement between the full theory model [16] and our effective model in calculating the energy of the Fermi polaron.

FINITE TEMPERATURE VARIATIONAL APPROACH FOR IMPURITY DYNAMICS

In order to model the dynamics of the Rabi oscillations and the impurity spectral response, we use the finite-temperature Truncated Basis Method (TBM) developed in Refs. [44, 54]. The basic details of this method are discussed in the main text. Our ansatz for the impurity operator is

$$\hat{c}(t) = \sum_\sigma \left[\alpha_0^\sigma(t)\hat{c}_{0\sigma} + \sum_{\mathbf{k}} \alpha_{\mathbf{k}}^\sigma(t)\hat{f}_{\mathbf{k}}^\dagger \hat{d}_{\mathbf{k}\sigma} + \sum_{\mathbf{k},\mathbf{q}} \alpha_{\mathbf{kq}}^\sigma(t)\hat{f}_{\mathbf{q}}^\dagger \hat{f}_{\mathbf{k}}\hat{c}_{\mathbf{q-k}\sigma} \right], \tag{S13}$$

where, for simplicity, we consider a vanishing total momentum. As discussed in the main text, we may quantify the error incurred in the Heisenberg equation of motion by introducing the error operator $\hat{\epsilon}(t) \equiv i\partial_t \hat{c}(t) - [\hat{c}(t), \hat{H}]$ and the associated error quantity $\Delta(t) \equiv \text{Tr}[\hat{\rho}_0 \hat{\epsilon}(t)\hat{\epsilon}^\dagger(t)]$. Using the minimization condition $\partial\Delta(t)/\partial\dot{\alpha}_j^{\sigma*}(t) = 0$ with respect to the variational coefficients $\{\alpha_j\}$, we arrive at

$$E\alpha_0^\uparrow = g_\uparrow \sum_{\mathbf{q}} \alpha_{\mathbf{q}}^\uparrow \text{Tr}\left[\hat{\rho}_0 \hat{f}_{\mathbf{q}}^\dagger \hat{f}_{\mathbf{q}}\right] + \frac{\Omega_0}{2}\alpha_0^\downarrow \tag{S14a}$$

$$(E - \varepsilon_{\mathbf{q}\uparrow})\alpha_{\mathbf{q}}^\uparrow = g_\uparrow \alpha_0^\uparrow + g_\uparrow \sum_{\mathbf{k}} \alpha_{\mathbf{kq}}^\uparrow \text{Tr}\left[\hat{\rho}_0 \hat{f}_{\mathbf{k}}\hat{f}_{\mathbf{k}}^\dagger\right] \tag{S14b}$$

$$(E - \varepsilon_{\mathbf{kq}})\alpha_{\mathbf{kq}}^\uparrow = g_\uparrow \alpha_{\mathbf{q}}^\uparrow + \frac{\Omega_0}{2}\alpha_{\mathbf{kq}}^\downarrow \tag{S14c}$$

$$(E - \Delta\omega)\alpha_0^\downarrow = g_\downarrow \sum_{\mathbf{q}} \alpha_{\mathbf{q}}^\downarrow \text{Tr}\left[\hat{\rho}_0 \hat{f}_{\mathbf{q}}^\dagger \hat{f}_{\mathbf{q}}\right] + \frac{\Omega_0}{2}\alpha_0^\uparrow \tag{S14d}$$

$$(E - \varepsilon_{\mathbf{q}\downarrow} - \Delta\omega)\alpha_{\mathbf{q}}^\downarrow = g_\downarrow \alpha_0^\downarrow + g_\downarrow \sum_{\mathbf{k}} \alpha_{\mathbf{kq}}^\downarrow \text{Tr}\left[\hat{\rho}_0 \hat{f}_{\mathbf{k}}\hat{f}_{\mathbf{k}}^\dagger\right] \tag{S14e}$$

$$(E - \varepsilon_{\mathbf{kq}} - \Delta\omega)\alpha_{\mathbf{kq}}^\downarrow = g_\downarrow \alpha_{\mathbf{q}}^\downarrow + \frac{\Omega_0}{2}\alpha_{\mathbf{kq}}^\uparrow. \tag{S14f}$$

Here we have taken the stationary condition since our Hamiltonian is time-independent,

$$\alpha_j^\sigma(t) = \alpha_j^\sigma(0)e^{-iEt} \equiv \alpha_j^\sigma e^{-iEt}, \tag{S15}$$

and defined $\varepsilon_{\mathbf{q}\sigma} \equiv \nu_\sigma - \epsilon_{\mathbf{q}}/2$ and $\varepsilon_{\mathbf{kq}} \equiv \epsilon_{\mathbf{q}-\mathbf{k}} + \epsilon_{\mathbf{k}} - \epsilon_{\mathbf{q}}$.

Equation (S14) represents a set of linear integral equations that define the time dependence of the variational coefficients $\{\alpha_j\}$. It is quite similar to the corresponding set of equations derived in Refs. [44, 54]. However, here we account for temperature, initial-state interactions, and the Rabi coupling between the two impurity spin states. Diagonalizing Eq. (S14) yields eigenvectors $\{\alpha_j^{(l)}\}$ and corresponding eigenvalues E_l. In what follows it is useful to write the eigenvectors as the union of the spin-$\uparrow$ and spin-$\downarrow$ components, i.e., $\{\alpha_j^{(l)}\} = \{\alpha_j^{\uparrow(l)}\} \cup \{\alpha_j^{\downarrow(l)}\}$.

The solutions of Eq. (S14) allow us to obtain stationary impurity operators

$$\hat{\phi}^{(l)} \equiv \sum_j \alpha_j^{(l)} \hat{O}_j, \tag{S16}$$

where the impurity basis operators $\{\hat{O}_j\} = \{\hat{c}_{\mathbf{0}\uparrow}, \hat{f}_{\mathbf{k}}^\dagger \hat{d}_{\mathbf{k}\uparrow}, \hat{f}_{\mathbf{q}}^\dagger \hat{f}_{\mathbf{k}} \hat{c}_{\mathbf{q}-\mathbf{k}\uparrow}, \hat{c}_{\mathbf{0}\downarrow}, \hat{f}_{\mathbf{k}}^\dagger \hat{d}_{\mathbf{k}\downarrow}, \hat{f}_{\mathbf{q}}^\dagger \hat{f}_{\mathbf{k}} \hat{c}_{\mathbf{q}-\mathbf{k}\downarrow}\}$ are those introduced in Eq. (S13). These all satisfy $\mathrm{Tr}\left[\hat{\rho}_0 \hat{O}_j \hat{O}_k\right] = 0$ when $j \neq k$, since the trace is over medium-only states. This in turn allows us to normalize the stationary solutions according to

$$\mathrm{Tr}\left[\hat{\rho}_0 \hat{\phi}^{(l)} \hat{\phi}^{(m)\dagger}\right] = \delta_{lm}. \tag{S17}$$

Using this, the impurity annihilation operator in Eq. (S13) can be expressed as

$$\hat{c}(t) = \sum_l \mathrm{Tr}\left[\hat{\rho}_0 \hat{c}(0) \hat{\phi}^{(l)\dagger}\right] \hat{\phi}^{(l)} e^{-iE_l t} = \sum_l \alpha_0^{(l)*} \hat{\phi}^{(l)} e^{-iE_l t}, \tag{S18}$$

where the initial impurity operator $\hat{c}(0) = \hat{c}_{\mathbf{0}\downarrow}$. We take a bare impurity as the initial state even though there are initial-state interactions, since the simulations yield essentially the same result as when we use a weakly interacting polaron. We presume this is because the weakly interacting polaron forms quickly (on a time scale set by $a_{3D\downarrow}^2$ in 3D) once we start the dynamics.

Finally, we discuss the character of the medium-only states appearing in Eq. (S14). Assuming that the interactions between the initial $\downarrow$ impurity and the medium particles are negligible (as is the case in the experiments [14, 16]), we may take the medium states to be thermal eigenstates at temperature T. Therefore, we have

$$\mathrm{Tr}\left[\hat{\rho}_0 \hat{f}_{\mathbf{q}}^\dagger \hat{f}_{\mathbf{q}}\right] \equiv \left\langle \hat{f}_{\mathbf{q}}^\dagger \hat{f}_{\mathbf{q}} \right\rangle_\beta = n_F(\epsilon_{\mathbf{q}}) \tag{S19}$$

where β is the inverse temperature and n_F is the Fermi-Dirac distribution function:

$$n_F(\epsilon_{\mathbf{q}}) \equiv \mathrm{Tr}\left[\hat{\rho}_0 \hat{f}_{\mathbf{q}}^\dagger \hat{f}_{\mathbf{q}}\right] = \frac{1}{e^{\beta(\epsilon_{\mathbf{q}} - \mu)} + 1}. \tag{S20}$$

The chemical potential μ is related to the medium density n via

$$n = \sum_{\mathbf{q}} n_F(\epsilon_{\mathbf{q}}) = \begin{cases} -\left(\frac{m}{2\pi\beta}\right)^{3/2} \mathrm{Li}_{3/2}(-e^{\beta\mu}) & \text{(3D)} \\ \frac{m}{2\pi\beta} \ln\left(1 + e^{\beta\mu}\right) & \text{(2D)} \end{cases} \tag{S21}$$

where Li is the polylogarithm. The density is related to the Fermi energy via

$$E_F = \frac{k_F^2}{2m} = \begin{cases} \frac{(6\pi^2 n)^{2/3}}{2m} & \text{(3D)} \\ \frac{4\pi n}{2m} & \text{(2D)} \end{cases} \tag{S22}$$

Impurity spectral function

In the limit of a weak Rabi coupling, we can obtain the spin-$\uparrow$ impurity spectral function within linear response:

$$A_\uparrow(\omega) \simeq \sum_l |\alpha_0^{\uparrow(l)}|^2 \delta(\omega - E_l), \tag{S23}$$
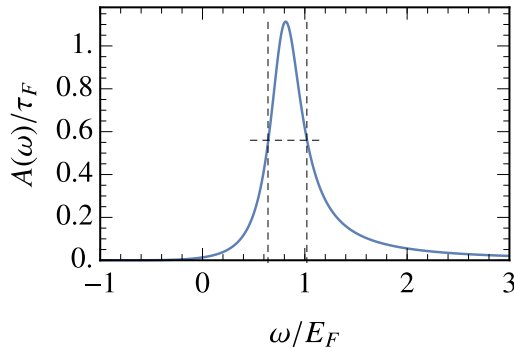
FIG. S3. Example of the calculation of the uncertainty in the detuning of Rabi oscillations onto the repulsive polaron. We show the spectral function of the repulsive polaron in the 2D ^{173}Yb experiment of Ref. [16] (solid line), with the dashed lines indicating the full-width half-maxima. The detuning is set between these half-maxima, leading to the uncertainty shown in Fig. 2 in the main text. The shown spectral function is for $\ln(1/k_F a_{2\mathrm{D}}) = 0.41$, $k_F R_{2\mathrm{D}} = 0.69$ and $T/T_F = 0.16$.

where the variational equations in Eq. (S14) are solved at $\Omega_0 = 0$. In practice, the spin-$\downarrow$ impurity interacts weakly with the medium, and thus the spectral function can be measured by driving transitions from the initial (nearly) non-interacting spin-$\downarrow$ impurity state into the spin-$\uparrow$ state. Indeed, this has been done in both experiments [14, 16].

Since the solution of Eq. (S14) are discrete, we convolve the resulting spectrum with a Gaussian to yield

$$I(\omega) = \sum_l |\alpha_0^{\uparrow(l)}|^2 g(\omega - E_l). \tag{S24}$$

Convolution of the spectrum in this case has the added benefit of enabling one to approximately model the finite duration of the pulses used in experiment.

Simulating Rabi oscillations

The Rabi oscillations are defined by

$$\mathcal{N}_\downarrow(t) = \left\langle \hat{c}(t) \hat{n}_\downarrow \hat{c}^\dagger(t) \right\rangle_\beta. \tag{S25}$$

We will take as our initial condition that $\hat{c}(t) = \hat{c}_{\mathbf{0}\downarrow}$, i.e., the impurity is initially in a bare spin-$\downarrow$ state, which means that the impurity number is $\mathcal{N}_\downarrow + \mathcal{N}_\uparrow = 1$ at all times. The Rabi oscillations are then given by

$$\mathcal{N}_\downarrow(t) \simeq \mathrm{Tr}[\hat{\rho}_0 \hat{c}_\downarrow(t) \hat{n}_\downarrow \hat{c}_\downarrow^\dagger(t)] = \sum_j \left| \sum_l \alpha_0^{\downarrow(l)*} e^{-iE_l t} \alpha_j^{\downarrow(l)} \right|^2. \tag{S26}$$

With the exception of detuning, all of the parameters used to define the Rabi oscillations are provided from the relevant experiment. The detuning in experiment is set to address the repulsive polaron peak, and to match this procedure, we use a calculated detuning such that the Rabi oscillations address the theoretically obtained spin-$\uparrow$ repulsive polaron. Due to small but finite initial state interactions, this detuning must take into account the energy of the spin-$\downarrow$ impurities. This is achieved by assuming the spin-$\downarrow$ impurities exist as zero-momentum repulsive polarons with a narrow spectral width. Owing to this assumption, combined with thermal fluctuations, a finite density of impurities and experimental limitations, we place an uncertainty on the detuning (see Fig. S3). This requires that we simulate Rabi oscillations over the range of possible detunings. The parameters used in the simulations of the Rabi oscillations in Figs. 2 and 3 can be found in Table S1.

We find that the inclusion of initial state interactions leads to a small reduction in the damping of the Rabi oscillations. This can be understood from the fact that in the limit in which the spin states have equal interactions, spin-symmetry implies that the Rabi oscillations would be undamped and oscillate at the bare Rabi frequency.
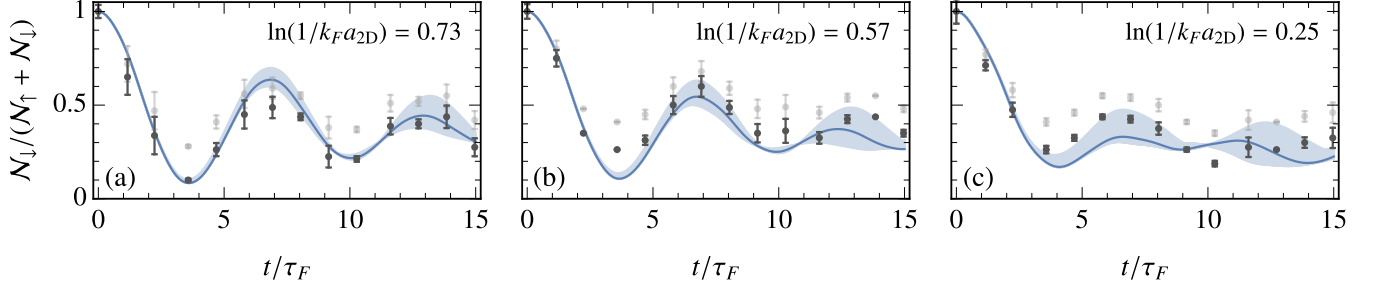
FIG. S4. Comparison of theory (blue solid lines) of Fig. 2(a)-(c) in the manuscript and the experimental data (black circles) with a constant offset of 0.2 removed and normalized to the value at time $t = 0$. The light-gray circles correspond to the unmodified data in the main text.

Finite offset in the Rabi oscillation measurement of the 2D experiment

As noted in the main text, there is a slight disagreement in the amplitude of the Rabi oscillations in the 2D experiment [16] and our variational approach. This disagreement can be explained with a constant offset $\epsilon > 0$ of the $\mathcal{N}_\downarrow$ measurement in the experiment. In our work, the relative population $\mathcal{N}_\downarrow/(\mathcal{N}_\downarrow + \mathcal{N}_\uparrow)$ of the 2D experiment is inferred from the sole measurement of $\mathcal{N}_\downarrow(t)$ and

$$\mathcal{N}_\downarrow/(\mathcal{N}_\downarrow + \mathcal{N}_\uparrow) \approx \mathcal{N}_\downarrow/[\mathcal{N}_\downarrow(t=0) + \mathcal{N}_\uparrow(t=0)] \approx \mathcal{N}_\downarrow/[\mathcal{N}_\downarrow(t=0) + 0] = \mathcal{N}_\downarrow/\mathcal{N}_\downarrow(t=0) . \tag{S27}$$

Thus, a constant offset in the measurement of $\mathcal{N}_\downarrow$ changes the relative population as

$$\mathcal{N}_\downarrow/\mathcal{N}_\downarrow(t=0) \rightarrow (\mathcal{N}_\downarrow + \epsilon)/[\mathcal{N}_\downarrow(t=0) + \epsilon] = \mathcal{N}_\downarrow/[\mathcal{N}_\downarrow(t=0) + \epsilon] + \epsilon/[\mathcal{N}_\downarrow(t=0) + \epsilon] , \tag{S28}$$

which directly shows how the mean of the relative population is artificially increased by $\epsilon/[\mathcal{N}_\downarrow(t=0) + \epsilon]$ and the amplitude is artificially reduced by the additional term ϵ in the denominator.

The offset ϵ in the experimental data originates from the detection method, for which the majority Fermi sea is removed, but a finite number of remaining majority atoms contributes a positive spurious signal to the measurement of $\mathcal{N}_\downarrow$. This contribution is independent of t and we estimate $\epsilon \lesssim 0.2\mathcal{N}_\downarrow$ from a reevaluation of the existing data of Ref. [16]. In Fig. S4, we illustrate how the removal of such an offset considerably improves the agreement between experiment and the variational approach. However, we have chosen not to subtract ϵ from the data in Fig. 2 of the main text as we lack a precise number for each data set.

TABLE S1. Parameters used for obtaining the theoretical curves and simulations shown in Figs. 2 and 3, matching the experimental ones from Refs. [16] and [14]. Experimental uncertainties are given in parenthesis were applicable. Note that the 3D effective range is always zero.

		Fig. 2						Fig. 3	
		(a)	(b)	(c)	(d)	(e)	(f)	(a), (c)	(b), (d)
Interaction parameter	$\ln(1/k_F a_{2D\uparrow})$	0.73(4)	0.57(5)	0.25(5)		—		0.07–0.91	—
	$\ln(1/k_F a_{2D\downarrow})$		4.9(1)			—		4.9(1)	—
	$1/k_F a_{3D\uparrow}$		—		2.63(4)	1.27(2)	0.22(1)	—	0.22–4.23
	$1/k_F a_{3D\downarrow}$		—		9.20(15)	6.94(11)	5.03(8)	—	5.03–11.43
Range parameter	$k_F R_{2D\uparrow}$	0.71	0.67	0.68		—		0.67–0.76	—
Rabi coupling	Ω_0/E_F	0.95(11)	0.96(11)	0.94(11)	0.68(1)	0.69(1)	0.67(1)	1.08	0.70
Reduced temperature	T/T_F		0.16(4)			0.13(2)		0.16(4)	0.13–0.14
Rep. polaron energy	$E_{+\uparrow}/E_F$	0.71	0.76	0.89	0.19	0.42	1.08	0.64–1.02	0.11–1.08
	$E_{+\downarrow}/E_F$		0.19		0.05	0.07	0.09	0.19	0.04–0.09
Detuning uncertainty	$\delta E_+/E_F$	0.24	0.31	0.47	0.02	0.05	0.42	0.19–0.65	0.02–0.42

GREEN'S FUNCTION APPROACH FOR QUASIPARTICLE PROPERTIES

A key alternative to our study of the impurity dynamics and properties in the TBM is provided through a Green's function approach. It has been shown that a variational approach using a single particle-hole excitation is equivalent to a Green's function approach calculated with non-self consistent T matrix theory — see Ref. [25] for a zero-temperature treatment, or Ref. [44] at finite temperature.

In this section, we take $\Omega_0 = 0$ in the variational equations (S14), while we consider the more general case in the next section. This allows us to derive a finite temperature impurity self energy $\Sigma_\sigma(E)$ separately within each of the impurity subspaces. Solving these equations for the energy then yields the expression

$$E = \sum_{\mathbf{q}} n_F(\epsilon_{\mathbf{q}}) \left[\frac{E - \varepsilon_{\mathbf{q}\sigma}}{g_\sigma^2} - \sum_{\mathbf{k}} \frac{1 - n_F(\epsilon_{\mathbf{k}})}{E - \varepsilon_{\mathbf{k}\mathbf{q}}} \right]^{-1}. \tag{S29}$$

The right hand side of this expression is precisely the impurity self energy at zero momentum using ladder diagrams at finite temperature [44]. The self energy is then related to the impurity (single-particle) Green's function through Dyson's equation,

$$G_\sigma(E) = \frac{1}{E - \Sigma_\sigma(E)}. \tag{S30}$$

The relevant properties of the repulsive polaron can now be defined in terms of the impurity self energy. In particular, the repulsive polaron energy $E_{+\sigma}$ is a (positive) solution to the implicit equation

$$\mathrm{Re}\left[\Sigma_\sigma(E)\right] = E. \tag{S31}$$

Expanding the Green's function around this pole, the repulsive polaron quasiparticle residue is

$$Z_\sigma = \left(1 - \frac{\partial\,\mathrm{Re}\left(\Sigma_\sigma(E)\right)}{\partial E}\bigg|_{E=E_{+\sigma}} \right)^{-1}, \tag{S32}$$

and the quasiparticle width is

$$\Gamma_\sigma = -Z_\sigma\,\mathrm{Im}\left[\Sigma_\sigma(E_{+\sigma})\right]. \tag{S33}$$

In addition to these properties, the impurity spectral function in Eq. (S23) is given by

$$A_\sigma(E) = -\frac{1}{\pi}\,\mathrm{Im}[G_\sigma(E)]. \tag{S34}$$

Repulsive polaron width at weak interactions

Here we provide details of the calculation of the approximate width of the repulsive polaron peak at weak interactions, Eq. (5). To perform this calculation, we specialize to three dimensions, zero temperature, and to a broad Feshbach resonance, i.e., $R_{3D} = 0$. In fact, the arguments in the following are valid as long as the thermal wavelength exceeds the scattering length while $R_{3D} \lesssim 1/(na_{3D}^2)$.

Assuming zero impurity momentum, the spin-↑ impurity self-energy in Eq. (S29) is given by (for simplicity, in this section we suppress all spin indices as well as "3D" subscripts)

$$\Sigma(E) = \sum_{\mathbf{q}} \Theta(k_F - q) \left[\frac{m}{4\pi a} - \left(\sum_{\mathbf{k}} \frac{1}{2\epsilon_{\mathbf{k}}} + \sum_{\mathbf{k}} \frac{1 - \Theta(k_F - k)}{E - \varepsilon_{\mathbf{k}\mathbf{q}} + i0} \right) \right]^{-1}. \tag{S35}$$

where $k \equiv |\mathbf{k}|$ and $q \equiv |\mathbf{q}|$ and we take the limit of $R_{3D} \to 0$, which according to Eq. (S7) is equivalent to taking the limit of $\nu, g \to \infty$ in such a way that

$$\frac{\nu}{g^2} = -\frac{m}{4\pi a} + \sum_{\mathbf{k}}^{\Lambda} \frac{1}{2\epsilon_{\mathbf{k}}}. \tag{S36}$$

We have also introduced a convergence factor $+i0$ which shifts the energy poles by an infinitesimal amount into the lower half of the complex plane.

In order to find the approximate form of the self-energy (and thereby the width) in the limit of weak interactions, we perturbatively expand the self-energy in scattering length (up to order a^2):

$$\Sigma(E) = \sum_{\mathbf{q}} \Theta(k_F - q) \left[\frac{4\pi a}{m} + \frac{16\pi^2 a^2}{m^2} \left(\sum_{\mathbf{k}} \frac{1}{2\epsilon_{\mathbf{k}}} + \sum_{\mathbf{k}} \frac{1 - \Theta(k_F - k)}{E - \varepsilon_{\mathbf{kq}} + i0} \right) \right]. \tag{S37}$$

In the limit of weak repulsive interactions, the repulsive polaron will have residue $Z \simeq 1$ and the width is thus given by

$$\Gamma \simeq -\mathrm{Im}[\Sigma(E_+)]. \tag{S38}$$

We can extract the imaginary component of the self-energy through the symbolic identity, which is valid for all real α:

$$\frac{1}{\alpha + i0} = \mathscr{P}\frac{1}{\alpha} - i\pi\delta(\alpha), \tag{S39}$$

where $\mathscr{P}$ denotes the Cauchy principal value. We thus have,

$$-\mathrm{Im}[\Sigma(E)] = \frac{16\pi^3 a^2}{m^2 E_F} \sum_{\mathbf{q},\mathbf{k}} \Theta(k_F - q)(1 - \Theta(k_F - k))\delta(E/E_F - \varepsilon_{\mathbf{kq}}/E_F). \tag{S40}$$

In the thermodynamic limit, these sums reduce to integrals that can be solved analytically in spherical coordinates:

$$-\mathrm{Im}[\Sigma(E)] = \frac{k_F^4 a^2}{16\pi m E_F^2} \left[4E^2 \ln\left(\frac{2E_F}{\sqrt{E_F(2E + E_F)} + E_F} \right) + 3E^2 - 4EE_F - 2E_F^2 + 2(E + E_F)\sqrt{E_F(2E + E_F)} \right]. \tag{S41}$$

Importantly, the imaginary part of the self energy is zero at zero energy, and we must therefore consider finite energy. In the limit of weak interactions, the energy of the repulsive polaron is given by the mean-field approximation [52]:

$$E_+ = \frac{2k_F^3 a}{3\pi m}. \tag{S42}$$

Using this energy and only retaining terms of order a^4 (the lowest non-zero contribution) the width is given by

$$\frac{\Gamma}{E_F} = \frac{8}{9\pi^3}(k_F a)^4. \tag{S43}$$

Since we originally expanded the self-energy up to order a^2 and have ended with a result that is of order a^4 we justify this result numerically in Fig. S5. Furthermore, we have checked that all contributions with multiple particle-hole excitations vanish at order a^4.

APPROXIMATE RABI OSCILLATIONS BASED ON GREEN'S FUNCTIONS

We finally turn to the arguments that led to Eq. (10) in the main text, which allowed us to link the repulsive polaron width to the damping of the Rabi oscillations. This will allow us to extend the standard approximation for extracting polaron properties from impurity Rabi oscillations [7]. It is useful to introduce a spectral decomposition of the Rabi oscillations, which is provided by the Fourier transform of Eq. (S26):

$$\mathcal{R}_{\downarrow}(\omega) \equiv \int dt\, e^{i\omega t} \mathcal{N}_{\downarrow}(t) \simeq \sum_{j,l,l'} \alpha_0^{\downarrow(l)^*} \alpha_j^{\downarrow(l)} \alpha_0^{\downarrow(l')} \alpha_j^{\downarrow(l')^*} \delta(\omega - E_l + E_{l'}). \tag{S44}$$
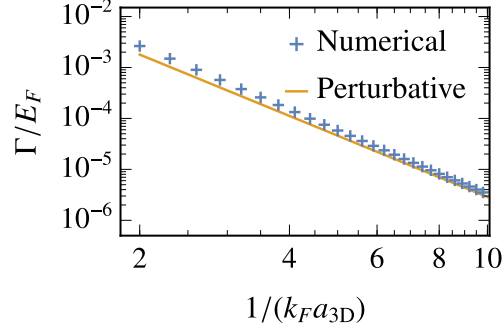
FIG. S5. Comparison of the perturbative expression for the repulsive polaron quasiparticle width in Eq. (S43) against the numerically exact calculation from Eq. (S33).

If the interactions are not too strong, the sum over intermediate states is dominated by the "bare" α_0 component, and thus

$$\mathcal{R}_\downarrow(\omega) \simeq \sum_{l,l'} |\alpha_0^{\downarrow(l)}|^2 |\alpha_0^{\downarrow(l')}|^2 \delta(\omega - E_l + E_{l'}). \tag{S45}$$

We thus recognize the Rabi spectrum as developing according to a convolution of spectral functions *in the presence of* Rabi coupling:

$$\mathcal{N}_\downarrow(t) \simeq \int d\omega \, d\omega' \, \tilde{A}_\downarrow(\omega) \tilde{A}_\downarrow(\omega') e^{-i(\omega-\omega')t}. \tag{S46}$$

Here

$$\tilde{A}_\downarrow(\omega) = -\frac{1}{\pi} \mathrm{Im}[\tilde{G}_\downarrow(\omega)], \tag{S47}$$

is calculated from the impurity Green's function including Rabi coupling.

We define the Rabi coupled Green's function $\tilde{G}$ via the exact relation

$$\tilde{G}(\omega) = \begin{pmatrix} G_\uparrow^{-1}(\omega) & \Omega_0/2 \\ \Omega_0/2 & G_\downarrow^{-1}(\omega) \end{pmatrix}^{-1}. \tag{S48}$$

For ease of notation, in the following we define $\tilde{G}_\downarrow(\omega) \equiv \tilde{G}_{22}(\omega)$. Approximating the decoupled Green's functions as

$$G_\sigma(\omega) \simeq \frac{Z_\sigma}{\omega - E_{+\sigma} - \delta_{\sigma\downarrow}\Delta\omega + i\Gamma_\sigma}, \tag{S49}$$

we find that

$$\mathcal{N}_\downarrow(t) \simeq Z_\downarrow^2 e^{-(\Gamma_\downarrow + \Gamma_\uparrow)t} \left[\frac{\Gamma_\uparrow - \Gamma_\downarrow}{\sqrt{\Omega_0^2 Z_\downarrow Z_\uparrow - (\Gamma_\uparrow - \Gamma_\downarrow)^2}} \sin\left(t\sqrt{\Omega_0^2 Z_\downarrow Z_\uparrow - (\Gamma_\uparrow - \Gamma_\downarrow)^2}\right) \right.$$
$$\left. + \left(1 - \frac{\Omega_0^2 Z_\downarrow Z_\uparrow}{2\Omega_0^2 Z_\downarrow Z_\uparrow - 2(\Gamma_\uparrow - \Gamma_\downarrow)^2}\right) \cos\left(t\sqrt{\Omega_0^2 Z_\downarrow Z_\uparrow - (\Gamma_\uparrow - \Gamma_\downarrow)^2}\right) + \frac{\Omega_0^2 Z_\downarrow Z_\uparrow}{2\Omega_0^2 Z_\downarrow Z_\uparrow - 2(\Gamma_\uparrow - \Gamma_\downarrow)^2} \right]. \tag{S50}$$

Here, we have taken $\Delta\omega = E_{+\uparrow} - E_{+\downarrow}$ for simplicity (i.e., on resonance Rabi oscillations). In the cases of interest where $Z_\downarrow$ is slightly below 1, the Rabi oscillations are not normalised. However, this is simply an artefact of our approximation of $G_\downarrow(\omega)$ and is overcome by dividing Eq. (S50) by $Z_\downarrow^2$.

Equation (S50) allows us to immediately identify the Rabi frequency and damping

$$\Omega \simeq \sqrt{\Omega_0^2 Z_\downarrow Z_\uparrow - (\Gamma_\uparrow - \Gamma_\downarrow)^2}, \tag{S51}$$

$$\Gamma_R \simeq \Gamma_\downarrow + \Gamma_\uparrow. \tag{S52}$$

These reduce to $\Omega \simeq \sqrt{\Omega_0^2 Z_\uparrow - \Gamma_\uparrow^2}$ and $\Gamma_R \simeq \Gamma_\uparrow$ in the case of weak initial state interactions. Equation (S51) illustrates why a strong Rabi coupling is necessary in order to drive coherent oscillations once $\Gamma_\uparrow$ becomes appreciable, which is why the oscillations are strongly suppressed for the strongest repulsive interactions in the 2D case (see Fig. 2). It also implies that we can estimate the quasiparticle residue by

$$Z_\uparrow \simeq \frac{\Omega^2 + \Gamma_\uparrow^2}{\Omega_0^2}. \tag{S53}$$

Finally, assuming weak initial state interactions such that $Z_\downarrow = 1$ and $\Gamma_\downarrow = 0$, and taking $\Omega_0 Z_\uparrow \gtrsim \Gamma_\uparrow$, we arrive at the form in Eq. (8) of the main text:

$$\mathcal{N}_\downarrow(t) \simeq e^{-\Gamma_\uparrow t} \left[\frac{1}{2} + \frac{1}{2} \cos \left(t\sqrt{\Omega_0^2 Z_\uparrow - \Gamma_\uparrow^2} \right) \right]. \tag{S54}$$

The limiting feature of this effective model comes from our approximation of $\hat{n}_\downarrow \simeq \hat{c}_{\mathbf{0}\downarrow}^\dagger \hat{c}_{\mathbf{0}\downarrow}$. For any $\Gamma_\uparrow, \Gamma_\downarrow > 0$, this approximation will always lead to $\mathcal{N}_\downarrow(t) \to 0$ for large t, which does not match the behaviour of Rabi oscillations in experiment or the TBM. However, at the intermediate times considered in Fig. 2 it provides a good model of the actual oscillations.